Femtosecond polarization spectroscopy: A density matrix description

L. D. Ziegler, R. Fan, and A. E. Desrosiers
Department of Chemistry, Boston University, Boston, Massachusetts 02215

N. F. Scherer[a)]
Department of Chemistry, University of Pennsylvania, Philadelphia, Pennsylvania 19104

(Received 20 August 1993; accepted 13 October 1993)

A density matrix treatment of the time evolution of the third order polarization response describing the optical heterodyne detected (OHD) transient birefringence and dichroism excited by ultrafast pulses is given. The relationship between frequency domain (Raman scattering) and time domain (pump–probe) spectroscopies is revealed by this pathway explicit description. Constructive and destructive interferences between time evolution density matrix pathways account for the respective strong birefringent and weak dichroic ground state nuclear response when the pulses are electronically nonresonant. However, for electronically resonant chromophores, the dichroic response is larger than the corresponding birefringent response due to constructive and destructive interferences respectively between density matrix time evolution histories. No such interferences contribute to spontaneous Raman scattering. The relative magnitude of the resonant dichroic and birefringent responses is pulse width dependent in the fast pulse limit and dependent on the relative rates of optical dephasing and ground state nuclear motion in the rapid optical dephasing limit. The spatial interpretation of the ground and excited state OHD polarization responses is given within the context of this polarization approach and the familiar Maker–Terhune notation. These relationships between time and frequency domain spectroscopies are illustrated by the observed OHD birefringence and dichroism and the spontaneous Raman spectra of both a nonresonant liquid (chloroform) and a resonant solution (I_2 in *n*-hexane).

I. INTRODUCTION

Impulsively excited quantum beats or coherences attributable to nuclear motions in ground or excited electronic states are a molecular response often detected in ultrafast pump–probe studies. Such beats are observed in spontaneous fluorescence,[1–3] impulsive stimulated scattering (ISS),[4,5] transmission correlation,[6,7] transient absorption,[8,9] and transient birefringence and dichroism[5,10–12] measurements and other four-wave mixing spectroscopies using ultrafast light pulses. The time dependence of these coherences, as well as the decay of the pump induced population, is a direct measure of both intra and intermolecular dynamics. Scherer *et al.* have recently reported the impulsively prepared optical heterodyne-detected (OHD) birefringence and dichroism of both electronically nonresonant liquids and resonant solutions.[13,14] OHD birefringence/dichroism may be described as polarization selective pump–probe spectroscopy. This technique allows the complex character of the third order polarization response to be separately observed by the choice of the relative local oscillator phase (*vide infra*). The OHD birefringence and dichroism, pumped and probed by 30 fs pulses resonant with the *B*-state absorption of I_2 in alkane solutions, unequivocally demonstrates the three types of *intra*molecular responses anticipated for resonant one-color pump–probe studies: excited state population and vibrational coherent superposition decay, and ground state vibrational coherent superposition decay. As discussed elsewhere,[13] the decays of the excited state contribution to these OHD responses establish the *B*-state predissociation lifetime as 200 fs in *n*-hexane (at 580 nm).

Mukamel and co-workers[15–18] have derived a general framework for the description of two-pulse pump–probe spectroscopies. The extension of this formalism to explicit optical phase sensitivity has also been considered and applied to the description of the OHD birefringence and dichroism experiments mentioned above.[19] This highly compact formalism is based on a nonlinear polarization density matrix description of pump–probe spectroscopy with well-separated pulses.

The total macroscopic third order polarization may equivalently be derived by summing over all possible time evolution histories of the bra/ket–radiation interactions.[20] Here we derive the OHD birefringence and dichroic signals due to electronically resonant and nonresonant ultrafast excitation based on such a density matrix approach where the explicit contributions of each distinct bra/ket time evolution history are considered separately. This pathway explicit approach provides a basis for qualitatively understanding the relative magnitudes of the pump–probe polarization measurements as well as a framework for a comparison of the various time and frequency domain P^3 or 4-wave mixing spectroscopies such as OHD birefringence, dichroism, ISS, RIKES, (resonance) Raman scattering and resonance fluorescence. In particular, the relationship between resonant and nonresonant Raman and OHD birefringence and dichroism is examined in detail here.

As for any sum-over-states or sum-over-time histories description of nonlinear spectroscopy, the relative phases

[a)]NSF—National Young Investigator.

 0021-9606/94/100(3)/1823/17/$6.00

of the various contributions may significantly affect the observed intensities. Interferences between the bra/ket evolution pathways have been shown to play a significant role in the description of several frequency domain spectroscopies. For example, density matrix interferences are central to the analysis of the spectrum of resonant secondary radiation, i.e., resonance Raman and resonance fluorescence emission,[21–23] and account for the appearance of extra features in resonant CARS spectra.[24] Such interferences are shown here to play a crucial role in determining the complex character of the third order polarization amplitude and hence the relative magnitude of transient birefringent and dichroic responses.

The analysis of electronically resonant OHD birefringence and dichroism will be analytically considered here for two pulse duration limits: (i) when the pulse duration is much shorter than the dephasing time of the resonant optical transition, and (ii) when the optical dephasing rate is faster than the pulse duration. For the short-pulse resonance condition (i), the relative strengths of the birefringence and dichroism is shown to be pulse width dependent. In addition, the pathway explicit approach given here allows a simple spatial interpretation for the various ground and excited state intramolecular responses observed in these OHD signals.

The expressions and relationships between time (OHD polarization pump–probe) and frequency domain (Raman) spectroscopies derived here are compared with experimental observations for both a nonresonant sample, chloroform, and a resonant chromophore, I_2 in *n*-hexane. Chloroform has two Raman active low frequency intramolecular modes at 262 and 369 cm^{-1} which are, respectively, depolarized and polarized bands and hence are both accessible via pump–probe studies with 30–60 fs pulses. The corresponding resonant Raman and resonant OHD birefringent/dichroic comparison will be shown for 580 nm pump–probe of 5 mM I_2 in *n*-hexane.

II. THEORY

A. A density matrix description of OHD birefringence and dichroism

1. General considerations

The pathway explicit contributions to the OHD polarization signals may be described in terms of the energy loss/gain of a probe field, called here the local oscillator field (LO), as a function of interpulse time delay (t_d) by[15]

$$W(t_d)^3 = -\int_{-\infty}^{\infty} P^3(t)\,\frac{\partial E_{\mathrm{LO}}}{\partial t}\,dt, \tag{1}$$

where

$$E_{\mathrm{LO}}(\phi) = (\eta E_0/2)e^{-t^2/2\tau^2}\{e^{i(\Omega t+\phi)} + e^{-i(\Omega t+\phi)}\}, \tag{2}$$

$$P^3(t) = \sum_{ab} P^3_{ab}(t) \quad \text{and} \quad P^3_{ab}(t) = \mu^*_{ab}\rho^3_{ab}(t) + \text{c.c.} \tag{3}$$

ϕ is the phase of the LO with respect to the probe pulse. $P^3(t)$ is the total third order macroscopic polarization that results from the sum over all the contributing third order polarization components, $P^3_{ab}(t)$, within the probe (detection) bandwidth. Each polarization contribution, $P^3_{ab}(t)$, represents a distinct or sum of distinct bra/ket time evolution histories as shown below.

Since several third order density matrix treatments of pump–probe spectroscopies have already been given[16,25–27] only the most salient features relevant to the OHD technique will be summarized here. The *n*th order density matrix element due to *n* radiation field interactions is represented by

$$\rho^n_{ab}(t) = \frac{i}{\hbar}\int_{-\infty}^{t} dt'\, R_{ab}(t-t')E(t')\rho^{n-1}_{aa}(t')\mu_{ab}. \tag{4}$$

$\rho^0_{ii} \equiv \rho^0_i$ is the initial ($t=-\infty$) population of level *i*. Throughout this treatment all molecular transition moments, μ_{ab}, will be taken to be time independent (effectively the Condon approximation, i.e., an electronic transition moment independent of nuclear motion) and the complex material response function will be given simply in the Bloch approximation form as

$$R_{ab}(t) = e^{-(i\omega_{ab}+1/T_{ab})t}. \tag{5}$$

Furthermore, all radiation fields will be described classically and be assumed to have a Gaussian pulse duration

$$E(t) = (E_0/2)e^{-t^2/2\tau^2}\{e^{i\Omega t} + e^{-i\Omega t}\}. \tag{6}$$

The probe LO field is chosen to be either in-phase ($\phi=0$) or 90° out-of-phase ($\phi=\pi/2$) with respect to the probe pulse for a measurement of the dichroic or birefringent response, respectively. Thus in the slowly varying amplitude approximation ($\Omega \gg 1/\tau$),

$$\begin{aligned}\frac{\partial E_{\mathrm{LO}}}{\partial t}(\phi=0) &= -\eta\Omega E_0 e^{-t^2/2\tau^2}\sin\Omega t,\\ \frac{\partial E_{\mathrm{LO}}}{\partial t}(\phi=\pi/2) &= -\eta\Omega E_0 e^{-t^2/2\tau^2}\cos\Omega t.\end{aligned} \tag{7}$$

ηE_0 is the adjustable LO amplitude. If the total third order polarization is expressed as the Fourier series component

$$\begin{aligned}P^3(t) &= \wp^3(t)e^{-i\Omega t} + \wp^3(t)^* e^{i\Omega t}\\ &= 2\,\mathrm{Re}\,\wp^3(t)\cos\Omega t + 2\,\mathrm{Im}\,\wp^3(t)\sin\Omega t\end{aligned} \tag{8}$$

then $\wp^3(t)$ is the complex scalar wave amplitude of the third order polarization at frequency Ω. Due to the phase selectivity of the LO, the birefringent and dichroic responses are thus proportional to the real and imaginary parts of the complex third order polarization amplitude $\wp^3(t)$, respectively [Eqs. (1), (7), and (8)].

2. Nonresonant pump–probe

When the pump frequencies are off-resonant with all electronic transitions, only the nuclear response of the ground electronic state contributes to the transient OHD polarization signals ($t_d > \tau$).[16,17,20] The third order polarization created by two nonresonant ultrafast pulses with interpulse delay greater than the pulse duration is given by the sum of two distinct bra/ket time evolution pathways. These two histories, referred to here as pathways I and II,

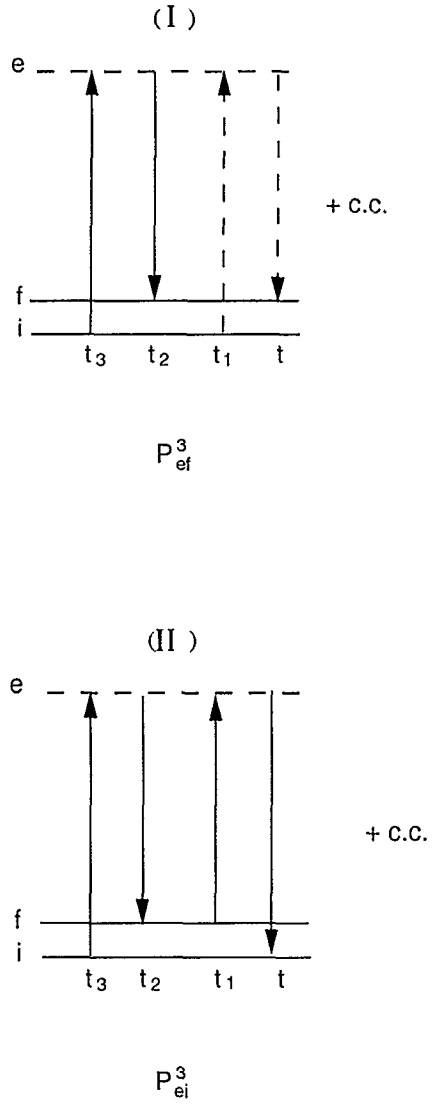

FIG. 1. The two density matrix time evolution pathways that contribute to the ground state nuclear response of the optical heterodyne detected (OHD) birefringence and dichroism of an electronically nonresonant material. Solid and dashed arrows correspond to bra and ket side time evolution. Time is increasing from left to right in each diagram. Path I contributes to nonresonant Raman scattering. Path II contributes to CARS.

are pictured in Fig. 1 for the three-level (electronically) nonresonant i,e,f molecular system. In pathway I, the initial bra (ket) $\langle i|$ is first polarized to state $\langle f|$ at second order and then the remaining ket (bra) is promoted to $|e\rangle$ which results in the third order polarization, P^3_{ef}. Within the rotating wave approximation, this is the time evolution history that accounts for nonresonant Raman scattering and the Raman component of resonant secondary radiation.[21,22] In pathway II, after the ground state coherence ρ^2_{if} is created by the first pulse, the probe pulse prepares the third order polarization P^3_{ie} by promoting the original bra (ket) to virtual level e (see Fig. 1). This is a time evolution history that contributes to ground state CARS signals.[20] Note that the original ket (bra) is unexcited as the bra (ket) solely undergoes the electric field driven evolution in pathway II. For these nonresonant pump–probe signals, pathway I results in the $i \rightarrow f$ material population change (inelastic or active spectroscopic change) whereas pathway II returns the system to the original population level (elastic or passive spectroscopic event).

When the optical dephasing constant of the off-resonant electronic transition is neglected relative to the detuning from resonance ($\omega_{ei}-\Omega > 1/T_2$) and the rotating wave approximation is assumed, the path specific mean energy loss/gain of the dichroic LO field is given by

$$W(t_d,\phi=0)=\frac{-\eta K\Omega}{\Delta^2}\,G(\omega_{fi})e^{-t_d/T_{2v}}\cos\omega_{fi}t_d \quad \text{Path I}, \tag{9}$$

$$W(t_d,\phi=0)=\frac{\eta K\Omega}{\Delta(\Delta-\omega_{fi})}\,G(\omega_{fi})e^{-t_d/T_{2v}}\cos\omega_{fi}t_d \quad \text{Path II}. \tag{10}$$

The corresponding nonresonant birefringent responses for each of the two possible bra/ket time evolution pathways are

$$W(t_d,\phi=\pi/2)=\frac{\eta K\Omega}{\Delta^2}\,G(\omega_{fi})e^{-t_d/T_{2v}}\sin\omega_{fi}t_d \quad \text{Path I} \tag{11}$$

$$W(t_d,\phi=\pi/2)=\frac{\eta K\Omega}{\Delta(\Delta-\omega_{fi})}\,G(\omega_{fi})e^{-t_d/T_{2v}}\sin\omega_{fi}t_d \quad \text{Path II}, \tag{12}$$

$$K=\frac{|\mu_{ei}|^2|\mu_{ef}|^2}{8\hbar^3}\,\rho^0_i E_0^4, \quad \Delta=\omega_{ei}-\Omega,$$

and

$$G(\omega_{fi})=2\pi\tau^2 e^{-\omega^2_{fi}\tau^2} \quad (\text{for } \tau < T_{2v} \text{ and } t_d > \tau). \tag{13}$$

T_{2v} is the total dephasing time constant of the ground electronic state vibrational coherence. For off-resonant pulses, $\Delta \simeq \Delta-\omega_{fi}$, and hence the pathway explicit OHD contributions are in-phase or π out-of-phase with nearly equal amplitude for the birefringent and dichroic responses, respectively. Thus the magnitude of the off-resonant birefringent and dichroic responses is determined by alternatively constructive and destructive interferences between third order polarization contributions P^3_{ei} and P^3_{ef} arising from density matrix time evolution pathways II and I, respectively. Consequently, the transient nonresonant birefringence due to impulsive pump–probe pulses is much larger than the dichroic response.

When the electronic dephasing rate, $1/T_2$, is neglected with respect to the detuning Δ or $\Delta-\omega_{fi}$ *after* the sum of pathway I and II polarization contributions is evaluated [note Eqs. (43) and (44) below], the off-resonant OHD birefringence and dichroism responses for this three level system (RWA), including the initial thermal population of level f, are given by

$$W(t_d)^{\mathrm{bir}} = -\frac{I_{\mathrm{pu}} I_{\mathrm{pr}} \Omega |\mu_{ei}|^2 |\mu_{ef}|^2 (2\Delta - \omega_{fi})}{\epsilon_0^2 c^2 \hbar^3 \Delta^2 (\Delta - \omega_{fi})^2} \times e^{-\omega_{fi}^2 \tau^2} [\Delta \rho_f^0 - (\Delta - \omega_{fi}) \rho_i^0] \times \sin \omega_{fi} t_d e^{-t_d / T_{2v}^g}, \quad (14)$$

$$W(t_d)^{\mathrm{dic}} = \frac{I_{\mathrm{pu}} I_{\mathrm{pr}} \Omega |\mu_{ei}|^2 |\mu_{ef}|^2 \Delta}{\epsilon_0^2 c^2 \hbar^3 \Delta^2 (\Delta - \omega_{fi})^2} e^{-\omega_{fi}^2 \tau^2} (\rho_i^0 - \rho_f^0) \times \left[\frac{4}{T_2^2} + \omega_{fi}^2 \right]^{1/2} \sin\{\omega_{fi} t_d + \theta\} e^{-t_d / T_{2v}^g}, \quad (15)$$

where the integrated pulse energy flux is defined as (units of energy area^{-1} per pulse)

$$I = \epsilon_0 c \int_{-\infty}^{\infty} |E(t)|^2 \, dt = \pi^{1/2} \tau \epsilon_0 c E_0^2 / 2 \quad (16)$$

and $\theta = \arctan(\omega_{fi} T_2 / 2)$, ϵ_0 is the electric permittivity and $I_{\mathrm{pr}} = \eta I_{\mathrm{pu}}$. Hence, the intramolecular vibrational contribution to the nonresonant OHD birefringence [Eq. (14)] will appear as a damped sinusoidal response without any additional constant phase shift. The corresponding nonresonant dichroic response may be phase shifted with respect to the birefringence by θ. This phase shift is determined by the relative magnitudes of the vibrational frequency (ω_{fi}) and the optical dephasing time of the off-resonant electronic transition ($2/T_2$) in this RWA three-level treatment. If the off-resonant electronic contribution is neglected or if $\omega_{fi} \gg 2/T_2$, then $\theta \to \pi/2$ and

$$W(t_d)^{\mathrm{dic}} \sim \omega_{fi} \cos \omega_{fi} t_d e^{-t_d / T_{2v}^g}. \quad (17)$$

Thus the phase of the off-resonant dichroic response is sensitive to the damping dynamics of the nonresonant source of polarizibility or, in other words, this phase is dependent on the small but finite spectral overlap between the pulse and the weak tail of the off-resonance electronic transition(s). Hence, dynamics on both the ground or excited electronic state surfaces contribute to the nonresonant dichroic response. An analogous damping dependent contribution to the nonresonant OHD birefringence also occurs, however, it is weaker by a factor of T_2^{-1}/Δ than the sinusoidal birefringence response [Eq. (14)] given above [see Eqs. (43)]. The relative importance of this excited state contribution to the off-resonant dichroism as compared to the corresponding birefringence is due to the destructive and constructive interferences, respectively, between pathways I and II polarization contributions discussed above. It should also be noted that these results are derived within the Condon approximation and the non-Condon effects, not considered here, may affect the phase of the observed OHD signals particularly for nontotally symmetric modes.

The relative magnitude of the OHD nonresonant birefringence [Eq. (14)] and dichroism [Eq. (15)] is given by the ratio of the off-resonance detuning (Δ) to the vibrational quantum (ω_{fi}) or the optical dephasing constant ($2/T_2$). Thus the OHD dichroic response is typically expected to be a few percent of the corresponding birefringent signal for most intramolecular responses of nonresonant samples. The dichroic and birefringent responses of chloroform excited by 30 fs pulses centered at 580 nm are shown in Fig. 2. These responses are obtained with the usual collinear pump–probe geometry. The standard optical heterodyne detection experimental arrangement as described elsewhere is employed here for these measurements.[11–13] As seen in this figure, the magnitude of the intramolecular ground state vibrational coherence contribution to the dichroic response is about 5% of that in the birefringent response. It should be noted that when $2/T_2 < \omega_{fi}$ the lowest frequency modes will be discriminated against in the dichroic signal due to the ω_{fi} vibrational frequency factor [Eq. (15)].

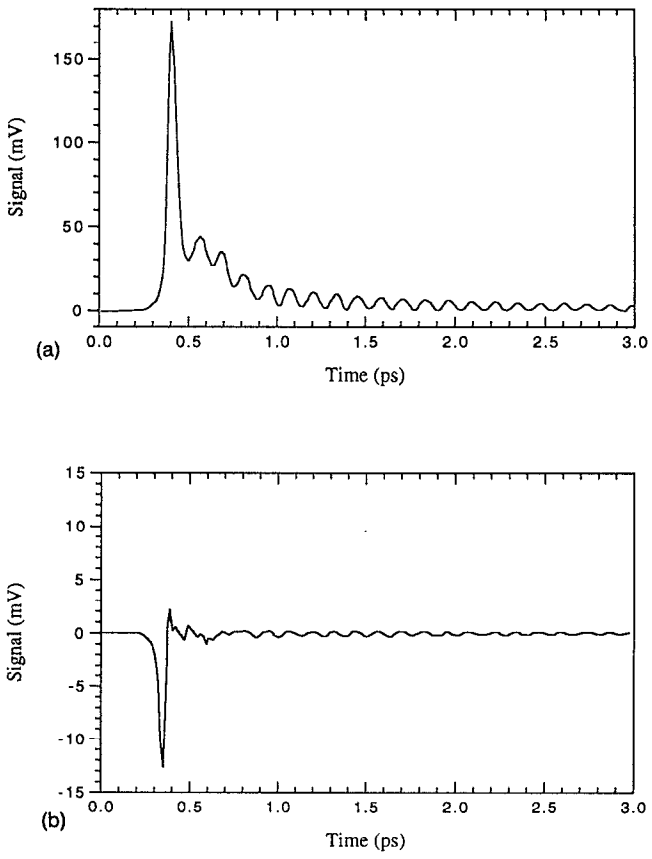

FIG. 2. The OHD (a) birefringence and (b) dichroism of $CHCl_3$ excited and probed by 30 fs pulses centered at 580 nm. The same LO field strength is used to obtain these two responses.

For off-resonant excitation, $\Delta \gg 1/T_2$, the birefringent response is consequently found to be proportional to the imaginary part of the nuclear response function $R(t)_{fi}$. When $\omega_{fi} > 1/T_2$, the real part of the nuclear response function $R(t)_{fi}$ is probed in the dichroic response. (Experimentally the $\omega_{fi} > 1/T_2$ condition can be verified by the observed phase shift.) Furthermore, as discussed above, the relative magnitudes of the real and imaginary parts of the complex polarization amplitude, $\wp(t)^3$, are due to constructive and destructive interferences between contributing density matrix time evolution histories (pathways I

and II) and *not* the real or imaginary parts of the corresponding path-specific susceptibilities alone.

In contrast to these vibrationally impulsive time domain polarization measurements, off-resonance Raman scattering cross section is proportional only to the imaginary part of $\wp(t)^3$ derived from density matrix pathway I alone. Hence the real part of the nuclear response function contributes directly to a spontaneous Raman scattering spectrum. Thus a more complete measure of the nuclear response function, at least for modes with $\omega_{fi} \geqslant \sim 50\ \mathrm{cm}^{-1}$, may be provided by a comparison of the dichroic and birefringent responses. These time domain measurements are analogous to the frequency domain OHD-RIKES technique[28–30] in terms of the ability of the LO phase to directly distinguish between the real and imaginary parts of the nuclear response function at least for intramolecular modes.

3. Electronically resonant OHD birefringence and dichroism

When the pump pulse is resonant with an electronic transition of a chromophore in the sample volume, additional intramolecular (and possibly intermolecular) responses in general appear in the birefringent and dichroic responses. Under resonance pump conditions the time dependence of both excited state population and vibrational coherences contribute to the OHD transient birefringence and dichroic signals in addition to the ground state vibrational response. In general, the phase and relative magnitude of these three responses will depend on the resonance detuning, pulse duration and optical dephasing rates. Expressions describing the relative magnitudes of the nuclear responses with respect to the LO phase, i.e., dichroism or birefringence, can be conveniently considered in two resonance limits (a) the short pulse/slow optical dephasing regime, $\tau < T_2$ and (b) long pulse/rapid optical dephasing limit, $T_2 < \tau$.

a. Short pulse/slow optical dephasing limit ($\tau < T_2$ and $t_d > \tau$). In the limit that the pulse duration (τ) is less than the optical dephasing time constant (T_2) of the resonant electronic transition, the intramolecular OHD dichroic responses originating in level i of the four level system pictured in Fig. 7 are given by

Dichroism

$$W(t_d)^{\mathrm{pop}} = -\frac{\eta\Omega E_0^4}{4\hbar^3} \sum_e |\mu_{ie}|^2 |\mu_{ef}|^2 \rho_i^0 \times \mathrm{Re}[G(-\Delta_{ei})L(\Delta_{ei})] \times \mathrm{Re}[G(\Delta_{ef})L(-\Delta_{ef})]e^{-t_d/T_1} \tag{18}$$

$$W(t_d)^{\mathrm{coh}}_{\mathrm{gnd}} = -\frac{\eta\Omega E_0^4}{4\hbar^3} \sum_{e,e'} \mu_{ie}\mu_{ef}\mu_{ie'}\mu_{e'i}\rho_i^0 \,\mathrm{Re}[G(\Delta_{e'f}) \times L(-\Delta_{e'i})][\{\mathrm{Re}[G(-\Delta_{ef})L(\Delta_{ei})]\}^2 + \mathrm{Im}[G(-\Delta_{ef})L(\Delta_{ei})]^2]^{1/2} \times \sin\{\omega_{fi}t_d + \Phi\}e^{-t_d/T^g_{2v}}, \tag{19}$$

where

$$\Phi = \arctan \frac{\mathrm{Re}[G(-\Delta_{ef})L(\Delta_{ei})]}{\mathrm{Im}[G(-\Delta_{ef})L(\Delta_{ei})]},$$

$$W(t_d)^{\mathrm{coh}}_{\mathrm{exc}} = -\frac{\eta\Omega E_0^4}{2\hbar^3} \sum_{e\neq e'} \mu_{ie}\mu_{ie'}\mu_{ef}\mu_{e'f}\rho_i^0 \times \mathrm{Re}[G(-\Delta_{ef})L(\Delta_{e'f})] \times \mathrm{Re}[G(-\Delta_{ei})L(\Delta_{e'i})]e^{-t_d/T^e_{2v}} \cos\omega_{e'e}t_d. \tag{20}$$

T_1, T^e_{2v}, T^g_{2v} are the excited state population, excited state vibrational ($\omega_{ee'}$) coherence and ground state (ω_{fi}) vibrational decay constants. The detuning parameters are $\Delta_{ei} = \omega_{ei} - \Omega$ and

$$G(\Delta_{ef})L(-\Delta_{e'f}) = \int_{-\infty}^{\infty} dt\, e^{-t^2/2\tau^2} e^{i\Delta_{ef}t} \int_{-\infty}^{t} dt_1 \times e^{-t_1^2/2\tau^2} e^{-i\Delta_{e'f}t_1}. \tag{21}$$

Correspondingly, when the LO pulse is $\pi/2$ shifted with respect to the probe pulse, the intramolecular birefringent responses of the electronically resonant chromophore in the short pulse/slow optical dephasing limit are given by

Birefringence

$$W(t_d)^{\mathrm{pop}} = -\frac{\eta\Omega E_0^4}{4\hbar^3} \sum_e |\mu_{ie}|^2 |\mu_{ef}|^2 \rho_1^0 \times \mathrm{Re}[G(-\Delta_{ei})L(\Delta_{ei})]\mathrm{Im}[G(\Delta_{ef}) \times L(-\Delta_{ef})]e^{-t_d/T_1}, \tag{22}$$

$$W(t_d)^{\mathrm{coh}}_{\mathrm{gnd}} = -\frac{\eta\Omega E_0^4}{4\hbar^3} \sum_{e,e'} \mu_{ie}\mu_{ef}\mu_{ie'}\mu_{e'f}\rho_i^0 \,\mathrm{Im}[G(\Delta_{e'f}) \times L(-\Delta_{e'i})][\{\mathrm{Im}[G(-\Delta_{ef})L(\Delta_{ei})]\}^2 + \mathrm{Re}[G(-\Delta_{ef})L(\Delta_{ei})]^2]^{1/2} \times \sin\{\omega_{fi}t_d + \Phi\}e^{-t_d/T^g_{2v}}, \tag{23}$$

$$W(t_d)^{\mathrm{coh}}_{\mathrm{exc}} = -\frac{\eta\Omega E_0^4}{2\hbar^3} \sum_{e\neq e'} \mu_{ie}\mu_{ie'}\mu_{ef}\mu_{e'f}\rho_i^0 \times \mathrm{Im}[G(-\Delta_{ef})L(\Delta_{e'f})]\mathrm{Re}[G(-\Delta_{ei}) \times L(\Delta_{e'i})]e^{-t_d/T^e_{2v}} \cos\omega_{e'e}t_d. \tag{24}$$

The relative magnitudes of the dichroic and birefringent responses in this short pulse limit are determined by the pulse duration and the detunings of the pump and probe carrier frequencies from electronic resonance. When the pulse convolution integral $G(\Delta)L(\Delta')$ is defined as above [Eq. (21)] the real and imaginary parts for near resonant short pulses can be approximated by (see the Appendix)

$$\mathrm{Re}\, G(\Delta)L(\Delta') \simeq (1-\Delta'^2\tau^2/2)(1-\Delta^2\tau^2/2)\pi\tau^2, \tag{25}$$

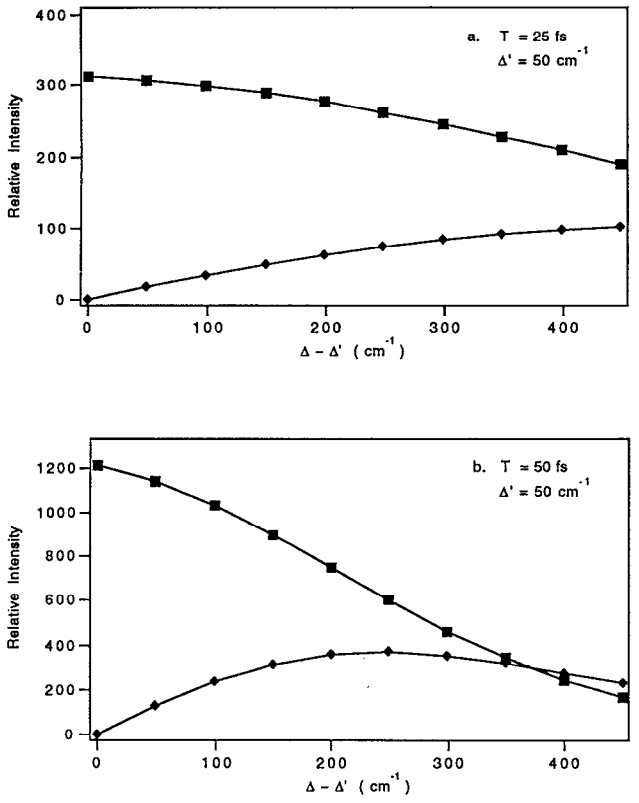

FIG. 3. Real (squares) and imaginary (diamonds) parts of Gaussian pulse integral $G(\Delta)L(\Delta')$ [defined by Eq. (21)] as a function of $\Delta-\Delta'$ for pulse durations (FWHH) of 25 and 50 fs.

$$\text{Im}\, G(\Delta)L(\Delta') \simeq (1-\Delta'^2\tau^2/2)(1-\Delta^2\tau^2/2) \times \pi^{1/2}\tau^3(\Delta-\Delta'), \tag{26}$$

thus

$$\frac{\text{Im}\, G(\Delta)L(\Delta')}{\text{Re}\, G(\Delta)L(\Delta')} \simeq \frac{\tau}{\pi^{1/2}}(\Delta-\Delta'). \tag{27}$$

As the pulse duration (τ) decreases, the contribution of Im $G(\Delta)L(\Delta')$ relative to Re $G(\Delta)L(\Delta')$ correspondingly decreases. Consequently, the relative magnitude of the resonant dichroic and birefringent responses is a function of the pump and probe pulse durations in this fast pulse limit [see Eqs. (18)–(20) and (22)–(24)]. In addition, the finite pulse duration, i.e., the relative real and imaginary character of the two-time integral $G(\Delta)L(\Delta')$, accounts for a small phase shift in the ground state responses. The real and imaginary parts of this function are plotted in Fig. 3 for two different pulse durations as a function of detunings from the pulse carrier frequency ($\Delta-\Delta'$). For the resonant OHD I_2 experiments referenced here using 30 fs pulses (FWHH), $\tau=12.8$ fs, $\Delta-\Delta'\sim\omega_{if}\sim 2\pi c(200\ \text{cm}^{-1})$, and hence Im $G(\Delta_{e'f})L(-\Delta_{e'i})$/Re $G(\Delta_{e'f})L(-\Delta_{e'i})\sim 0.3$. Thus for pulses of this duration ($\sim$30 fs) the resonant dichroic signals are larger than the corresponding resonant birefringent responses [compare Eqs. (18)–(20) with Eqs. (22)–(24)].

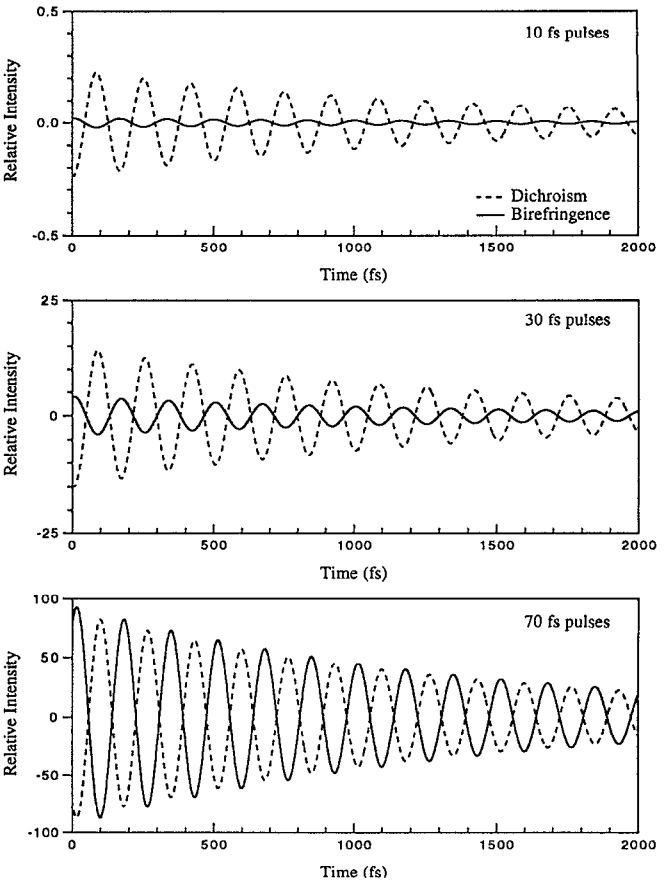

FIG. 4. Calculated resonant ($\Omega=\omega_{ei}$) OHD birefringence and dichroism signals due to a ground state vibrational coherence ($\omega_{fi}=200\ \text{cm}^{-1}$, $T^g_{2v}=1.4$ ps) as a function of pulse duration in the fast pulse limit ($\tau < T_2$). Relative intensity units are the same for each panel.

The effect of pulse duration on the relative dichroic and birefringent impulsive OHD responses in this fast pulse resonant limit is also demonstrated in Fig. 4. The contribution of a ground state vibrational coherence ($\omega_{fi}=200\ \text{cm}^{-1}$, $T^g_{2v}=1.4$ ps) to these signals due to resonant ($\Omega=\omega_{ei}$) pulses is shown for conserved pulse energy as a function of pulse duration. The dependence of the relative birefringence and dichroic signals, as well as a τ-dependent phase shift, is clearly evident in this figure as the pulse width is changed from 10 to 70 fs.

The relative magnitudes of the resonant OHD dichroism and birefringence can be more readily understood in terms of the component density matrix pathways contributing to the ground and excited state molecular responses. The density matrix evolution diagrams contributing to the ground state vibrational coherence response is shown in Fig. 5 (same as Fig. 1 except state e is real). The path specific contributions to the *resonant* ground state vibrational response originating in level i for the three level system ($e=e'$) are

Dichroism

Path I

$$W(t_d) = -K(a^2+b^2)e^{-t_d/T^g_{2v}}\cos\omega_{fi}t_d. \tag{28}$$

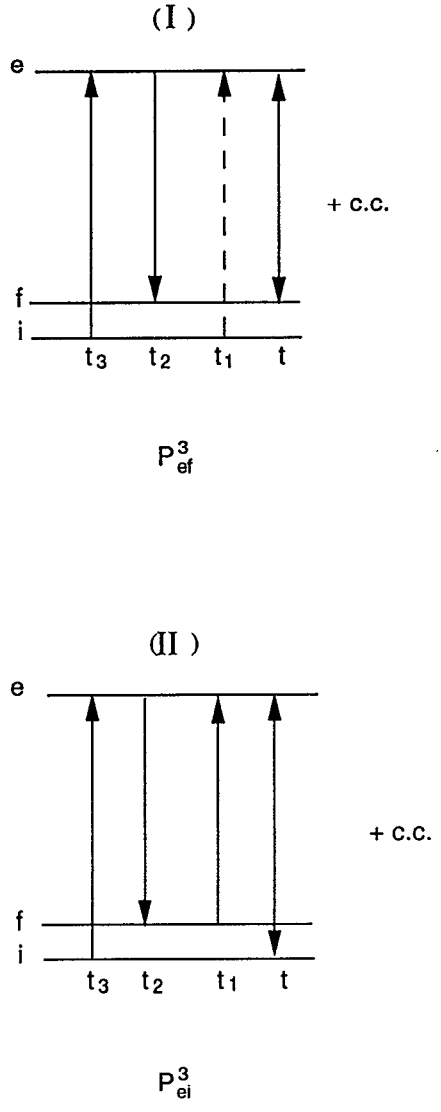

FIG. 5. The two density matrix time evolution pathways that contribute to the ground state nuclear response of the optical heterodyne detected (OHD) birefringence and dichroism of an electronically resonant three level system. Solid and dashed arrows correspond to bra and ket side time evolution. Time is increasing from left to right in each diagram. The last interaction is represented by a double sided arrow since the collapse of the third order polarization can result in population of either level e or f (path I) or e or i (path II).

Path II

$$W(t_d) = -K(a^2+b^2)e^{-t_d/T_{2v}^g}\sin(\omega_{fi}t_d+\alpha). \tag{29}$$

Birefringence

Path I

$$W(t_d) = K(a^2+b^2)e^{-t_d/T_{2v}^g}\sin\omega_{fi}t_d. \tag{30}$$

Path II

$$W(t_d) = K(a^2+b^2)e^{-t_d/T_{2v}^g}\cos(\omega_{fi}t_d+\alpha), \tag{31}$$

where

$$K = \eta\Omega E_0^4|\mu_{ie}|^2|\mu_{fe}|^2\rho_i^0/8\hbar^3, \tag{32}$$

$$a = \mathrm{Re}[G(-\Delta_{ef})L(\Delta_{ei})],$$

$$b = \mathrm{Im}[G(-\Delta ef)L(\Delta ei)],$$

and

$$\alpha = \arctan\left[\frac{a^2-b^2}{2ab}\right].$$

These pathway dependent polarization components to the resonant ($\Omega=\omega_{ei}$) birefringence and dichroism are plotted in Fig. 6 for the $\omega_{fi}=200\ \mathrm{cm}^{-1}$, $T_{2v}^g=1.4$ ps vibrational coherence and 10 and 70 fs pulse durations. In contrast to the *off-resonant* path specific intramolecular dichroic and birefringent responses [Eq. (9)–(12)], path I and path II derived polarizations, respectively, P_{ef}^3 and P_{ei}^3, *constructively* interfere for the resonant dichroic response and *destructively* interfere for the resonant birefringent response. Furthermore, these path dependent polarization components are phase shifted with respect to each other as a function of pulse width (see Fig. 6). Hence, the extent of this interference between time evolution pathways is consequently dependent on the pulse duration. Pathway II introduces a t_d independent phase shift to the resonant ground state responses in this fast pulse/slow optical dephasing limit [Eq. (31)].

Similarly, interfering contributions from different density matrix histories account for the relative magnitude of excited state coherences in resonant dichroic and birefringent responses. The density matrix evolution diagrams responsible for the excited state vibrational coherence signal are shown in Fig. 7. Pathways 1 and 4 contribute to $P_{e'f}^3$ and pathways 2 and 3 contribute to P_{ef}^3. The corresponding OHD dichroism and birefringence due to each of these polarizations are

Dichroism

$P_{e'f}^3$ Paths 1 and 4

$$W(t_d)_{\mathrm{exc}}^{\mathrm{coh}} = -K[a_i'(a_f'^2+b_f'^2)^{1/2}]e^{-t_d/T_{2v}^e}\sin(\omega_{e'e}t_d+\beta). \tag{33}$$

P_{ef}^3 Paths 2 and 3

$$W(t_d)_{\mathrm{exc}}^{\mathrm{coh}} = K[a_i'(a_f'^2+b_f'^2)^{1/2}]e^{-t_d/T_{2v}^e}\sin(\omega_{e'e}t_d-\beta). \tag{34}$$

Birefringence

$P_{e'f}^3$ Paths 1 and 4

$$W(t_d)_{\mathrm{exc}}^{\mathrm{coh}} = K[a_i'(a_f'^2+b_f'^2)^{1/2}]e^{-t_d/T_{2v}^e}\cos(\omega_{e'e}t_d+\beta). \tag{35}$$

P_{ef}^3 Paths 2 and 3

$$W(t_d)_{\mathrm{exc}}^{\mathrm{coh}} = K[a_i'(a_f'^2+b_f'^2)^{1/2}]e^{-t_d/T_{2v}^e}\cos(\omega_{e'e}t_d-\beta), \tag{36}$$

where

$$K = \eta\Omega E_0^4\mu_{ie}\mu_{ie'}\mu_{fe}\mu_{fe'}\rho_i^0/8\hbar^3, \tag{37}$$

$$a_i' = \mathrm{Re}[G(-\Delta_{ei})L(\Delta_{e'i})],$$

$$a_f' = \mathrm{Re}[G(-\Delta_{ef})L(\Delta_{e'f})],$$

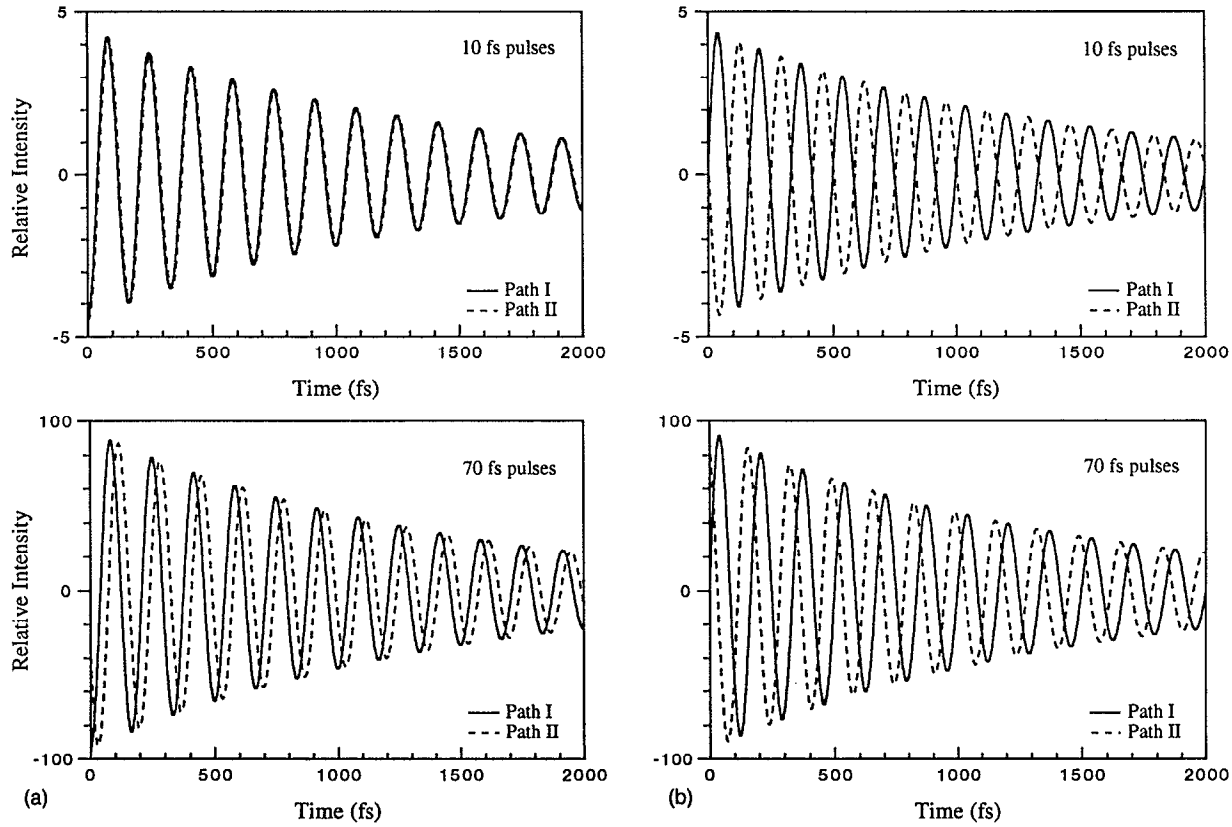

FIG. 6. The pathway I and II explicit OHD (a) dichroism and (b) birefringence contribution of an impulsively excited ground state vibrational (ω_{fi}=200 cm^{-1}, T^g_{2v}=1.4 ps) contribution for 10 and 70 fs pulses in the fast pulse resonant ($\Omega=\omega_{ei}$) limit. Paths I and II are defined in Fig. 1.

$$b'_f=\mathrm{Im}[G(-\Delta_{ef})L(\Delta_{e'f})],\quad \text{and}\quad \beta=\arctan(a'_f/b'_f).$$

The magnitude of the resonant excited state vibrational dichroic/birefringent response results from constructive/destructive interference between pathways leading to P^3_{ef} (pathways 2 and 3) and $P^3_{e'f}$ (pathways 1 and 4). This density matrix pathway interference is pulse duration dependent as shown above. Each of the path specific nuclear responses have identical amplitude but are symmetrically phase shifted with respect to each other. This phase shift is pulse duration and detuning dependent.

As Figs. 6 and 7 and Eqs. (25) and (26) reveal, the magnitude of both the birefringent as well as the dichroic responses will decrease as the pulse duration decreases (for a fixed electric field amplitude, E_0). Mathies *et al.* have pointed this out in the context of explicit wave packet calculations of P^3 responses.[27] In a delta function pulse limit $G(\Delta)L(\Delta')=1$, the destructive interferences between P^3_{ei} and P^3_{ef}, and between $P^3_{e'f}$ and P^3_{ef} will be complete and thus only the dichroic responses will be observed.

Finally, when the initial thermal population of level f is explicitly considered in this four level, fast pulse limit, the ground state vibrational coherence signals are given by

Dichroism

$$W(t_d)^{\mathrm{coh}}_{\mathrm{gnd}}=-\frac{\eta\Omega E_0^4}{4\hbar^3}\sum_{e,e'}\mu_{id}\mu_{ef}\mu_{ie'}\mu_{e'i}\,\mathrm{Re}[G(\Delta_{e'f})\times L(-\Delta_{e'i})]e^{-t_d/T^g_{2v}}[(\rho^0_i+\rho^0_f)\times\mathrm{Re}[G(-\Delta_{ef})L(\Delta_{ei})]\cos\omega_{ei}t_d+(\rho^0_i-\rho^0_f)\times\mathrm{Im}[G(-\Delta_{ef})L(\Delta_{ei})]\sin\omega_{fi}t_d]. \quad (38)$$

Birefringence

$$W(t_d)^{\mathrm{coh}}_{\mathrm{gnd}}=-\frac{\eta\Omega E_0^4}{4\hbar^3}\sum_{e,e'}\mu_{id}\mu_{ef}\mu_{ie'}\mu_{e'i}\,\mathrm{Im}[G(\Delta_{e'f})\times L(-\Delta_{e'i})]e^{-t_d/T^g_{2v}}[(\rho^0_i+\rho^0_f)\times\mathrm{Re}[G(-\Delta_{ef})L(\Delta_{ei})]\cos\omega_{ei}t_d+(\rho^0_i-\rho^0_f)\times\mathrm{Im}[G(-\Delta_{ef})L(\Delta_{ei})]\sin\omega_{fi}t_d]. \quad (39)$$

Thus the temperature dependence of ground state vibrational contributions to resonant birefringence and dichroism responses may be pulse width dependent.

b. Rapid optical dephasing limit ($T_2<\tau$). When the pulse width is long with respect to the optical dephasing decay of the resonant electronic transition, expressions for OHD polarization signals can also be analytically derived.

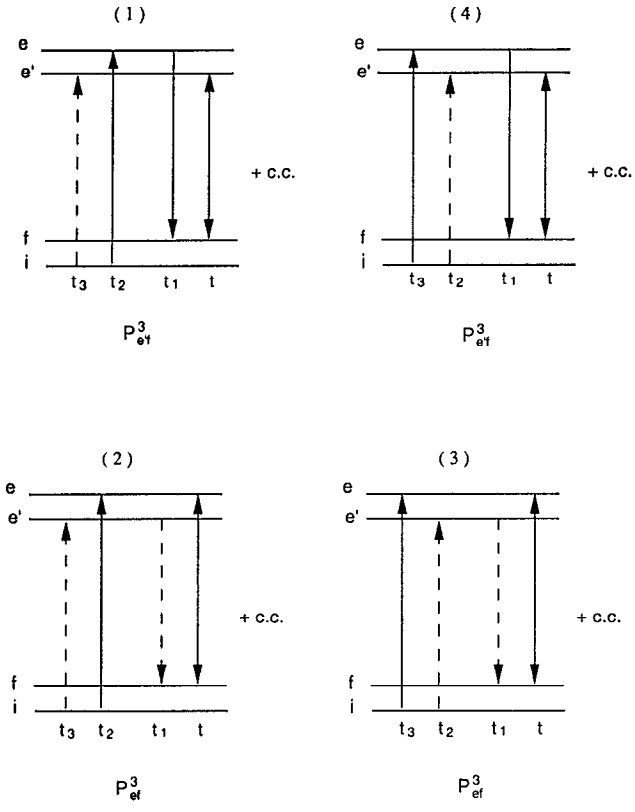

FIG. 7. Energy level diagrams describing the time evolution of the excited state coherence contribution to the resonant OHD detected birefringence and dichroism. Pathways 1 and 4 contribute to $P^3_{e'f}$ and pathways 2 and 3 contribute to P^3_{ef}. As in Fig. 4, solid and dashed arrows correspond to bra and ket side evolution and time is increasing from left to right.

In this limit the homogeneous width of the resonant electronic transition is broader than the spectral width of the pump/probe pulses. The population decay contributions to these responses for $t_d > \tau$ and pulse durations shorter than the molecular dynamics of interest ($\tau < T_1$) in the rapid dephasing limit are given by

Dichroism

$$W(t_d)^{\text{pop}} = -\frac{2\Omega I_{\text{pu}} I_{\text{pr}}}{\epsilon_0^2 c^2 \hbar^3} \sum_e \rho_i^0 |\mu_{ie}|^2 |\mu_{ef}|^2 \frac{\text{Re}\, e^{i\theta_1}}{r_1} \frac{\text{Re}\, e^{i\theta_2}}{r_2} \times e^{-t_d/T_1}. \tag{40}$$

Birefringence

$$W(t_d)^{\text{pop}} = \frac{2\Omega I_{\text{pu}} I_{\text{pr}}}{\epsilon_0^2 c^2 \hbar^3} \sum_e \rho_i^0 |\mu_{ie}|^2 |\mu_{ef}|^2 \frac{\text{Re}\, e^{i\theta_1}}{r_1} \frac{\text{Im}\, e^{i\theta_2}}{r_2} \times e^{-t_d/T_1}, \tag{41}$$

$$\tan\theta_1 = (\Delta_{ei})/(1/T_2); \quad \tan\theta_2 = (\Delta_{ef})/(1/T_2),$$

$$r_1^2 = \Delta_{ei}^2 + 1/T_2^2; \quad r_2^2 = \Delta_{ef}^2 + 1/T_2^2. \tag{42}$$

When the pulse duration is longer than the optical dephasing time but shorter than the nuclear dynamics of interest, the relative contribution of the population decay to the dichroic and birefringent responses of this three level system is given by: $W(t_d)^{\text{dic}}/W(t_d)^{\text{bir}} = (\tan\theta_2)^{-1} = (1/T_2)/(\Omega - \omega_{ef})$. If the pump pulse is resonant with the $i \rightarrow e$ transition, $\Omega - \omega_{ef} = \omega_{fi}$ and the relative magnitudes of the dichroism/birefringence signals are $\sim 1/T_2/\omega_{fi}$. Hence, in the limit of this rapid optical dephasing regime where $1/T_2 > \omega_{fi}$, the excited state population contribution to the dichroism signal will be larger than the corresponding birefringence.

The contribution of ground state vibrational coherences to the OHD polarization signal are given by the two bra/ket evolution pathways (I and II, Fig. 5) discussed above. When the initial population of ground state levels i and f are explicitly included, the resonant dichroic and birefringent responses due to both density matrix histories in this fast dephasing limit are

Dichroism

$$W(t_d)^{\text{coh}}_{\text{gnd}} = \frac{\Omega I_{\text{pu}} I_{\text{pr}}}{\epsilon_0^2 c^2 \hbar^3 r_1^2 r_2^2} e^{-\omega_{fi}^2 \tau^2} |\mu_{ei}|^2 |\mu_{ef}|^2 e^{-t_d/T_{2v}^g} \times \left[\frac{(2\Delta_{ei} - \omega_{fi})}{T_2} (\rho_f^0 - \rho_i^0) \sin\omega_{fi} t_d - \{2(\rho_f^0 + \rho_i^0)/T_2^2 + (\rho_f^0 - \rho_i^0)\Delta_{ei}\omega_{fi} + \rho_i^0 \omega_{fi}^2\} \cos\omega_{fi} t_d \right] \tag{43}$$

Birefringence

$$W(t_d)^{\text{coh}}_{\text{gnd}} = -\frac{\Omega I_{\text{pu}} I_{\text{pr}}}{\epsilon_0^2 c^2 \hbar^3 r_1^2 r_2^2} e^{-\omega_{fi}^2 \tau^2} |\mu_{ei}|^2 |\mu_{ef}|^2 e^{-t_d/T_{2v}^g} \times (2\Delta_{ei} - \omega_{fi}) \left[\frac{\rho_i^0 + \rho_f^0}{T_2} \cos\omega_{fi} t_d + \{\Delta_{ei}\rho_f^0 - (\Delta_{ei} - \omega_{fi})\rho_i^0\} \sin\omega_{fi} t_d \right]. \tag{44}$$

The expressions for the off-resonant OHD polarization response given above [Eqs. (14) and (15)] are obtained from this more general result when $1/T_2$ is neglected with respect to Δ, the off-resonance detuning. In general, the phase of this ground state coherence and the relative magnitudes of the dichroic and birefringent responses will depend on the detunings (Δ_{ei}, Δ_{ef}), optical dephasing rate and ground state vibrational frequency as shown above in this pulse limit [Eqs. (43) and (44)]. However, when the pump pulse is resonant with the $i \rightarrow e$ electronic transition, i.e., $\Delta_{ei} = 0$, and in this fast optical dephasing limit, we take $1/T_2 > \omega_{fi}$, the dichroic and birefringent responses reduce to

Dichroism

$$W(t_d)^{\text{coh}}_{\text{gnd}} = -\frac{2\Omega I_{\text{pu}} I_{\text{pr}}}{\epsilon_0^2 c^2 \hbar^3 (1/T_2)^2} e^{-\omega_{fi}^2 \tau^2} |\mu_{ei}|^2 |\mu_{ef}|^2 e^{-t_d/T_{2v}^g} \times (\rho_f^0 + \rho_i^0) \cos\omega_{fi} t_d. \tag{45}$$

Birefringence

$$W(t_d)^{\rm coh}_{\rm gnd}=\frac{2\Omega I_{\rm pu}I_{\rm pr}}{\epsilon_0^2c^2\hbar^3(1/T_2)^3}\,e^{-\omega_{fi}^2\tau^2}|\mu_{ei}|^2|\mu_{ef}|^2e^{-t_d/T^g_{2v}}$$
$$\times(\rho^0_f+\rho^0_i)\omega_{fi}\cos\omega_{fi}t_d. \tag{46}$$

The relative magnitude of the above dichroic and birefringent responses is again given by $1/T_2/\omega_{fi}$. Thus under these resonance conditions ($T_2<\tau$, $1/T_2>\omega_{fi}$, and $\Omega=\omega_{ei}$), the dichroic response will be larger than the birefringent response and these signals will exhibit π shifted cosinusoidal oscillations. This effect is due to the constructive (destructive) interference between pathway I and II density matrix contributions to the resonant dichroic (birefringent) response. In this rapid dephasing resonance limit, if $1/T_2\sim\omega_{fi}>\tau^{-1}$ the two time evolution pathways, I and II, cancel much less completely. Consequently, the transient dichroism and birefringence will be of the same order of magnitude and a t_d independent phase shift will be observed.

The excited state vibrational coherence contributions in the rapid dephasing limit to the OHD dichroism and birefringence are given by

Dichroism

$$W(t_d)^{\rm coh}_{\rm exc}=-\frac{\Omega I_{\rm pu}I_{\rm pr}}{\epsilon_0^2c^2\hbar^3}\,\rho^0_ie^{-\omega_{ee'}^2\tau^2}\mu_{ie}\mu_{ie'}\mu_{ef}\mu_{e'f}e^{-t_d/T^e_{2v}}$$
$$\times\left[\frac{\cos(-\theta_2-\theta_1'-\omega_{e'e}t_d)}{r_1'r_2}\right.$$
$$+\frac{\cos(\theta_1'-\theta_2'+\omega_{e'e}t_d)}{r_1'r_2'}$$
$$+\frac{\cos(-\theta_2'-\theta_1+\omega_{e'e}t_d)}{r_2'r_1}$$
$$\left.+\frac{\cos(\theta_2-\theta_1-\omega_{e'e}t_d)}{r_2r_1}\right]. \tag{47}$$

Birefringence

$$W(t_d)^{\rm coh}_{\rm exc}$$
$$=-\frac{\Omega I_{\rm pu}I_{\rm pr}}{\epsilon_0^2c^2\hbar^3}\,\rho^0_ie^{-\omega_{ee'}^2\tau^2}\mu_{ie}\mu_{ie'}\mu_{ef}\mu_{e'f}e^{-t_d/T^e_{2v}}$$
$$\times\left[\frac{\sin(-\theta_2-\theta_1'-\omega_{e'e}t_d)}{r_1'r_2}+\frac{\sin(\theta_1'-\theta_2'+\omega_{e'e}t_d)}{r_1'r_2'}\right.$$
$$\left.+\frac{\sin(-\theta_2'-\theta_1+\omega_{e'e}t_d)}{r_2'r_1}+\frac{\sin(\theta_2-\theta_1-\omega_{e'e}t_d)}{r_2r_1}\right], \tag{48}$$

$$r_1'^2=(\Delta_{e'i})^2+1/T_2^2;\quad r_2'^2=(\Delta_{e'f})^2+1/T_2^2;$$
$$\tan\theta_1'=\Delta_{e'i}/(1/T_2);\quad \tan\theta_2'=\Delta_{e'f}/(1/T_2). \tag{49}$$

The four cosine/sine terms in the dichroic/birefringent responses above correspond sequentially to the density matrix evolution histories labeled 1, 2, 3, and 4 in Fig. 7. If we consider the limit where the optical dephasing rate is greater than the relevant detunings, i.e., $1/T_2\gg\omega_{e'i}-\Omega$, as might be anticipated in the rapid optical dephasing limit, then $\theta_{1,2}$ and $\theta'_{1,2}\simeq 0$, and Eqs. (47) and (48) reduce to

Dichroism

$$W(t_d)^{\rm coh}_{\rm exc}\simeq-\frac{4\Omega I_{\rm pu}I_{\rm pr}}{\epsilon_0^2c^2\hbar^3(1/T_2)^2}\,\rho^0_ie^{-\omega_{ee'}^2\tau^2}\mu_{ie}\mu_{ie'}\mu_{ef}\mu_{e'f}$$
$$\times e^{-t_d/T^e_{2v}}\cos\omega_{e'e}t_d. \tag{50}$$

Birefringence

$$W(t_d)^{\rm coh}_{\rm exc}\simeq 0. \tag{51}$$

Thus in the resonant limit where the homogenous linewidth ($1/T_2$) is larger than detunings ω_{ei}, $\omega_{e'i}-\Omega$, and ω_{ef}, $\omega_{e'f}-\Omega$ ($\theta_{1,2}\simeq 0,\theta'_{1,2}\simeq 0$) the excited state vibrational coherence contribution to the birefringence is vanishingly small compared to the corresponding dichroic response. As can be seen in Eqs. (47) and (48), when $\theta_{1,2}$, $\theta'_{1,2}=0$ the polarization components due to paths 1 and 4, and 2 and 3 (Fig. 7) constructively and destructively interfere for the dichroic and birefringent excited state vibrational coherence response, respectively. These results are in contrast with the conclusions of Ref. 11 where the resonant birefringence and dichroism responses were attributed to ground and excited state dynamics, respectively.

The amplitudes of the population and ground and excited state vibrational coherence nuclear responses have distinct pulse width dependences. The population decay signals [Eqs. (40) and (41)] are just proportional to the integrated pulse energies, at least for pulse durations less than the excited state dynamics of interest ($\tau<T_1$). However, the magnitude of the ground and excited state vibrational coherence contributions to the OHD polarization signals [Eqs. (43), (44) and (47), (48)] is a maximum for pulse durations of ω_{fi}^{-1} and $\omega_{e'e}^{-1}$, respectively. Thus in this rapid optical dephasing limit, the population decay terms may be much larger than contributions from a particular Raman active mode for pulse durations (τ) significantly smaller or greater than the corresponding period of this mode. The analysis presented above is strictly given for a four level system. Generalization to multivel treatments, particularly necessary for cases of large electron–phonon coupling, is straightforward.

4. Spatial interpretation of time-domain OHD birefringence and dichroism

In order to make a quantitative comparison of time and frequency domain third order polarization dependent spectroscopies, the spatial dependence of the pump–probe electric field polarizations must be considered. The macroscopic nonlinear material polarization response in the ith direction due to three active electric fields polarized along the j,k,l space fixed directions may be described using the third order susceptibility elements χ^3_{ijkl}. In the familiar Maker–Terhune notation where the field frequencies obey $\Omega=\Omega_1+\Omega_2+\Omega_3$ (and the k-vector dependence is suppressed) we have[29–31]

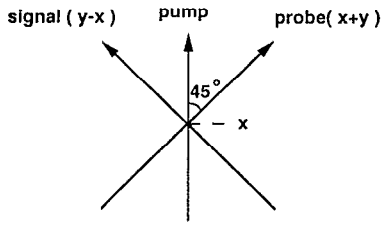

FIG. 8. Orientation of the linear polarized electric field vectors of the pump, probe, and signal fields for the OHD birefringent and dichroic measurements.

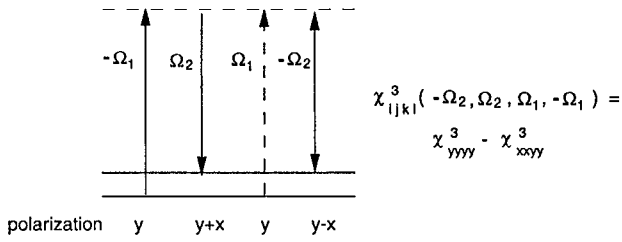

FIG. 9. Polarization direction explicit density matrix diagrams corresponding to frequency domain optical Kerr effect (OKE) or Raman induced Kerr effect (RIKES) measurements.

$$P_i^3(\Omega)=\chi^3_{ijkl}(-\Omega,\Omega_1,\Omega_2,\Omega_3)E_j(\Omega_1)E_k(\Omega_2)E_l(\Omega_3). \tag{52}$$

Equivalently, in the time domain[31]

$$P_i^3(t)=\int dt_1\int dt_2\int dt_3\,\chi^3_{ijkl}(t,t_1,t_2,t_3) \times E_j(t_1)E_k(t_2)E_l(t_3). \tag{53}$$

The time and frequency domain susceptibilities are related by the appropriate Fourier transform relationships. For purposes of this discussion χ^3_{ijkl} can represent either the time or frequency explicit dependent susceptibility as long as the pairing of the time or frequency arguments and the spatial indices is preserved.[31] Here we will adopt the field ordering convention used by Hellwarth $\chi^3_{ijkl}(-\Omega_2,\Omega_2,\Omega_1,-\Omega_1)$ for two beam dependent P^3 spectroscopies.[31] In isotropic media there are four nonvanishing susceptibility elements ($ijkl$=1111, 1122, 1212, and 1221) and they obey the relationship: 1111=1122+1212+1221. The 1 and 2 subscripts on χ^3 represent mutually perpendicular polarization directions.

a. Nonimpulsive pump-probe polarization spectroscopies. The differential polarized ($\|$) and depolarized ($\perp$) cross sections of spontaneous Raman scattering can be described by terms that contribute to the imaginary part of $\chi^3(-\Omega_2,\Omega_2,\Omega_1,-\Omega_1)$ and the isotropic (iso) and anisotropic (aniso) parts of the Raman scattering tensor by[28,29]

$$\left(\frac{d\sigma}{d\Omega}\right)_{\|} \propto \mathrm{Im}\,\chi^3_{1111}(-\Omega_2,\Omega_2,\Omega_1,-\Omega_1) \propto \mathrm{iso}+\tfrac{4}{3}\,\mathrm{aniso}, \tag{54a}$$

$$\left(\frac{d\sigma}{d\Omega}\right)_{\perp} \propto \mathrm{Im}\,\chi^3_{2211}(-\Omega_2,\Omega_2,\Omega_1,-\Omega_1) = \mathrm{Im}\,\chi^3_{1221}(-\Omega_2,\Omega_2,\Omega_1,-\Omega_1) \propto \mathrm{aniso}. \tag{54b}$$

Ω_1 and Ω_2 are the linearly polarized incident and scattered field frequencies, respectively.

The nonlinear polarization description of the optical field induced birefringence (optical Kerr effect) and its Raman resonant version (RIKES) are well known in the cw or nonimpulsive limit, i.e., where no vibrational coherences are directly prepared by the Ω_1 or Ω_2 incident beams alone. In the typical optical Kerr effect geometry shown in Fig. 8, the anisotropy created by a linearly polarized pump beam is probed by a second beam with its electric polarization vector oriented at 45° with respect to the pump and a new polarization component perpendicular to the probe is detected. The active susceptibility elements describing this material response may be discerned from the corresponding density matrix evolution diagram shown in Fig. 9. If Ω_1 and Ω_2 are the pump and probe frequencies, respectively, then the OKE or RIKES signal is proportional to[30]

$$S^{\mathrm{OKE/RIKES}} \propto \chi^3_{1212}(-\Omega_2,\Omega_2,\Omega_1,-\Omega_1) + \chi^3_{1221}(-\Omega_2,\Omega_2,\Omega_1,-\Omega_1), \tag{55a}$$

$$= \chi^3_{1111}(-\Omega_2,\Omega_2,\Omega_1,-\Omega_1) - \chi^3_{1122}(-\Omega_2,\Omega_2,\Omega_1,-\Omega_1). \tag{55b}$$

The observed OKE response thus arises from the *difference* between refractive indices parallel and perpendicular to the pump polarization direction. Correspondingly, the RIKES signal is proportional to the difference between polarized and depolarized Raman scattering cross sections of the mode at $\Omega_1-\Omega_2$. In terms of the Raman scattering polarizability tensor components, S^{RIKES} is thus proportional to iso+1/3 aniso.[28] These relationships hold for electronic resonance as well as off-resonance excitation.

b. OHD polarization spectroscopy with ultrafast pulses. Pump–probe measurements of the transient birefringence and dichroism due to ultrafast pulses capable of impulsive or coherent vibrational excitation are represented by the density matrix time evolution diagrams shown in Fig. 10. The relative polarizations of the pump, probe, and detection/signal fields are the same as described above in Fig. 8. In contrast to cw OKE/RIKES measurements the fields creating the ground state vibrational coherence have the same polarization in the femtosecond polarization experiments [compare Figs. 9 and 10(a)]. The impulsively excited ground state vibrational contribution to the OHD transient birefringent or dichroic response is given by [see Fig. 10(a)]

$$S_g^{\mathrm{coh}} \propto \chi^3_{1221}(-\Omega_2,\Omega_2,\Omega_1,-\Omega_1) + \chi^3_{1122}(-\Omega_2,\Omega_2,\Omega_1,-\Omega_1) \propto \mathrm{aniso}. \tag{56}$$

Thus in contrast to the frequency domain RIKES spectra, the contributions of impulsively excited ground state

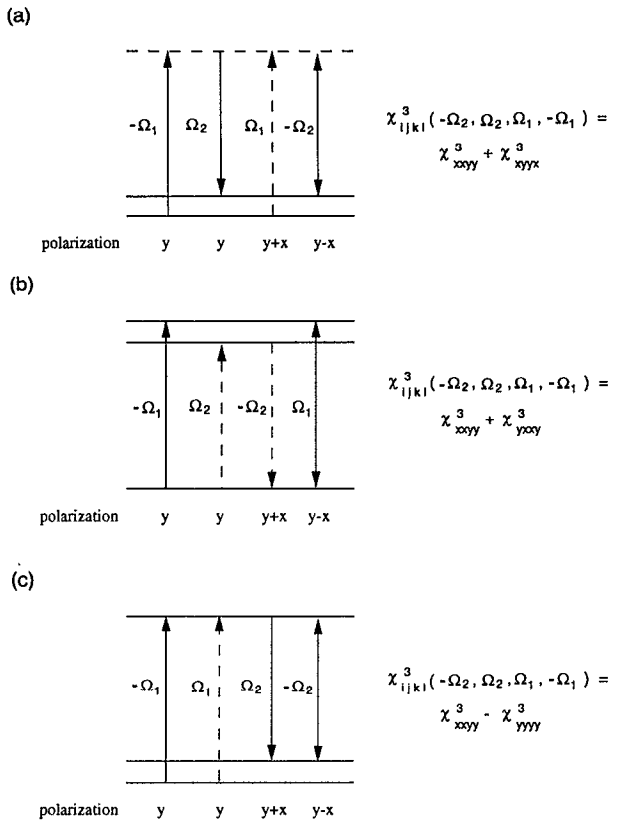

FIG. 10. Polarization direction explicit density matrix diagrams corresponding to the OHD time domain experiments. (a) Ground state vibrational coherence; (b) excited state vibrational coherence; and (c) excited state population.

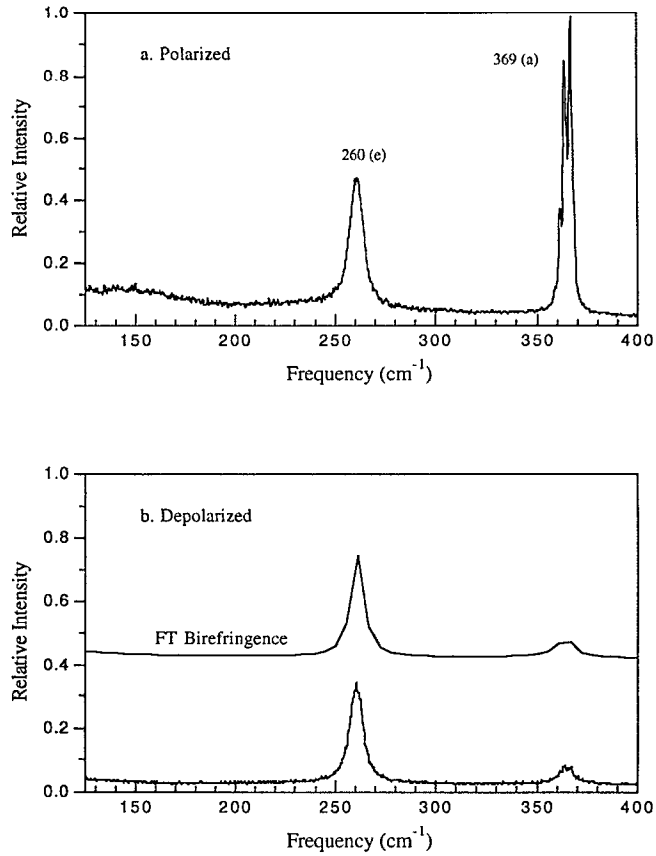

FIG. 11. Polarized and depolarized spontaneous Raman spectrum of chloroform excited by cw radiation at 580 nm. The imaginary part of the Fourier transform of the OHD birefringence excited by 30 fs pulses at 580 nm is shown in the lower panel.

Raman coherences to the OHD time resolved birefringent and dichroic responses are exclusively proportional to the anisotropic part of the Raman scattering polarizability tensor.

Excited state vibrational coherences appear in these transient polarization responses when the pump pulse is electronically resonant as described above. A corresponding density matrix time evolution diagram is shown in Fig. 10(b). The active susceptibility elements governing this contribution may be deduced from this diagram and are thus found to be

$$S_e^{\rm coh} \propto \chi^3_{1221}(-\Omega_2,\Omega_2,\Omega_1,-\Omega_1) + \chi^3_{1122}(-\Omega_2,\Omega_2,\Omega_1,-\Omega_1) \propto \text{aniso.} \quad (57)$$

Thus in analogy to the ground state Raman OHD response, the impulsive excited state contributions are proportional to the anisotropic part of the two-photon tensor corresponding to the Raman scattering of the *excited electronic state* vibrational mode due to resonance with the $e \rightarrow g$ transition.

The density matrix time evolution of the excited state population component to the resonant OHD signals is described by diagrams of the type shown in Fig. 10(c). In contrast to the impulsive vibrational OHD transient responses, the excited state population OHD resonant dichroic and birefringent responses are proportional to

$$S_e^{\rm pop} \propto \chi^3_{1221}(-\Omega_2,\Omega_2,\Omega_1,-\Omega_1) + \chi^3_{1212}(-\Omega_2,\Omega_2,\Omega_1,-\Omega_1), \quad (58a)$$

$$= \chi^3_{1111}(-\Omega_2,\Omega_2,\Omega_1,-\Omega_1) - \chi^3_{1122}(-\Omega_2,\Omega_2,\Omega_1,-\Omega_1). \quad (58b)$$

The excited state population contribution to the OHD signals arises from the differential absorption/stimulated emission of the probe beam, i.e., 1111–1122. Thus the origin of the population decay response in the ultrafast transient regime is identical to that of the cw, i.e., nonimpulsive, OKE or RIKES spectra as described above.[30]

III. COMPARISON OF TIME AND FREQUENCY DOMAIN POLARIZATION DEPENDENT SIGNALS

A. Nonresonant excitation

The polarized and depolarized spontaneous Raman spectra of chloroform excited at 580 nm are shown in Fig. 11. The two intramolecular $CHCl_3$ modes at 261 cm^{-1} (e) and 365 cm^{-1} (a) are clearly observed to be depolarized and polarized, respectively. The relative intensity (by peak height) of the 261 cm^{-1}/365 cm^{-1} modes is 6.5±0.5 in

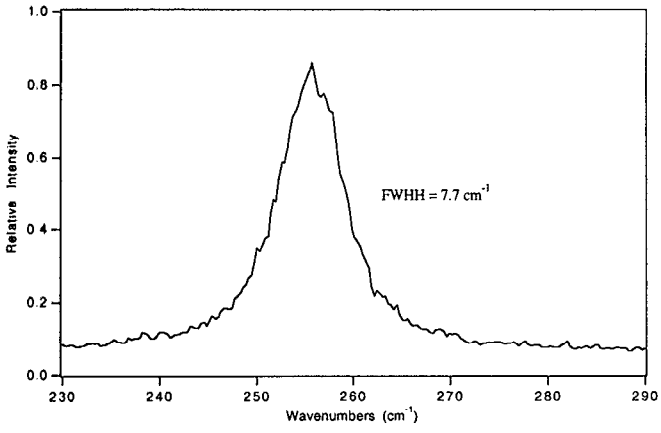

FIG. 12. Depolarized Raman spectrum of the 260 cm^{-1} band of $CHCl_3$. The 7.7 cm^{-1} bandwidth corresponds to 1.4 ps dephasing time.

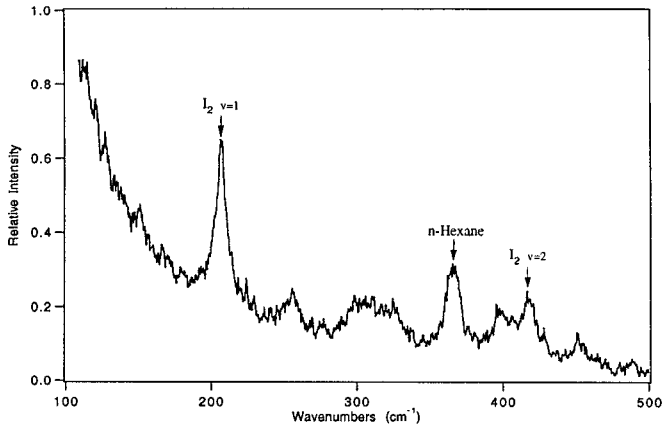

FIG. 13. The depolarized spontaneous resonance Raman spectrum of 5 mM I_2 in *n*-hexane excited at 580 nm. The I_2 fundamental (210 cm^{-1}), first overtone (420 cm^{-1}), and an *n*-hexane band (370 cm^{-1}) are indicated. The other weaker features are solvent bands.

the depolarized Raman spectrum. The imaginary part of the Fourier transform of the transient OHD birefringence of chloroform pumped and probed by 30 fs pulses centered at 580 nm (Fig. 2) and corrected by the autocorrelation of the pulses is compared to the depolarized spontaneous Raman spectrum in Fig. 11(b). In agreement with the analysis presented above, the relative intensities of the two intramolecular chloroform Raman active modes are identical in the birefringence FT and the *depolarized* spontaneous Raman spectrum.

The predicted off-resonant interpulse delay dependence of the birefringent response is $\exp(-t_d/T_{2v})\sin\omega_{fi}t_d$ [Eq. (15)]. Furthermore, this signal is proportional to the anisotropic part of the Raman scattering tensor as demonstrated above. Thus the imaginary part of the Fourier transform of the birefringent response should correspond to a Lorentzian with a linewidth (FWHH) equal to that of the *depolarized* spontaneous Raman spectrum. From a singular value decomposition fit of the observed birefringence to a sum of exponentially damped cosinusoidal functions the oscillations corresponding to the 261 cm^{-1} mode decay with an exponential time constant of 1.4 ps. The observed linewidth (FWHH) of this band in the depolarized Raman scattering spectrum is 7.7 ± 0.2 cm^{-1} (Fig. 12). This corresponds to a total dephasing time of $1.4\pm.04$ ps in excellent agreement with the time domain results. Thus the time dependence of the nonresonant OHD polarization signals are seen to be proportional to the FT of the anisotropic part of the ground state Raman scattering tensor in agreement with the discussion above. Furthermore, the homogeneous part of the anisotropic Raman linewidth is often taken as the product of purely rotational and vibrational dephasing components.[32] Such a model is consistent with the form of the signal interpulse delay dependence [$S(t_d)$] previously assumed for the analysis of the OHD polarization responses, i.e., $S(t_d)=R(t_d)W(t_d)$ where the rotational reorientation and vibrational coherence decay are $R(t_d)$ and $W(t_d)$, respectively.[13,20]

B. Relation of OHD responses to the resonance Raman spectrum

The depolarized spontaneous resonance Raman spectrum of 5 mM I_2 in *n*-hexane excited at 580 nm is shown in Fig. 13. Several bands are observed in the 100–500 cm^{-1} region. The I_2 fundamental (211 cm^{-1}) is the strongest vibrational feature and the 370 cm^{-1} band of *n*-hexane is the next most intense band. The first vibrational overtone of I_2 and several other solvent bands are also clearly evident. The corresponding OHD resonant birefringence and dichroism of 5 mM I_2 in *n*-hexane pumped and probed by 30 fs pulses at 580 nm are shown in Figs. 14 and 15. The nuclear responses obtained by subtracting the early time electronic response are shown in Fig. 14 insets. The I_2 responses dominate the resonant dichroic signal (Fig. 15) but are barely evident in the resonant birefringent response (Fig. 14). In the Fourier transform of the dichroic response the I_2 fundamental and first overtone are clearly seen, however, the *n*-hexane fundamental, the second most intense feature in the resonance Raman spectrum (Fig. 13) is not detected in the resonant dichroism (Fig. 15).[13] By contrast *n*-hexane nuclear responses dominant the birefringence of the I_2 resonant solution (Fig. 14).

These effects are due to the interferences between the contributing bra/ket time evolution histories as described above. The resonant I_2 dichroic and birefringent responses are described by the fast pulse limit; $\tau=30$ fs, $T_2=200$ fs. In the *n*-hexane solution dichroism, the ground and excited state vibrational responses of the resonant solute (I_2) are derived from constructive interferences between density matrix evolution pathways I and II (Fig. 5) or between pathways 1 and 4, and 2 and 3 (Fig. 7), respectively. In contrast, destructive interferences between time evolution pathways eliminate the nonresonant solvent responses from the I_2 solution dichroism. However, density matrix pathways constructively interfere for the solvent and partially destructively interfere for the resonant solute (I_2) in the solution birefringence.The cw spontaneous resonance Raman spectrum or more exactly the Raman component

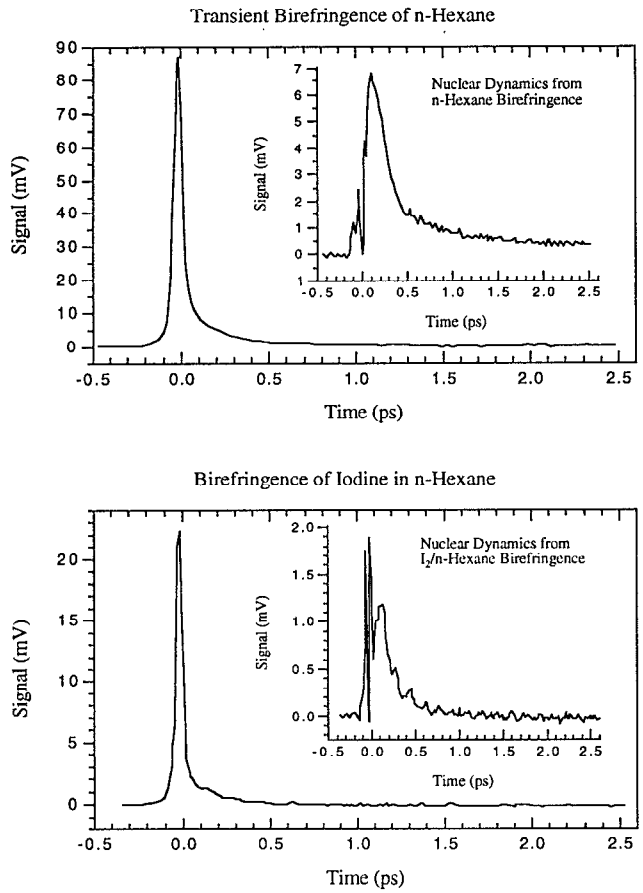

FIG. 14. The OHD birefringence of 5 mM I_2 in *n*-hexane and neat *n*-hexane excited by 30 fs pulses at 580 nm. The nuclear part of the OHD response, i.e., after removal of the shortest time electronic response, is given in the inset.

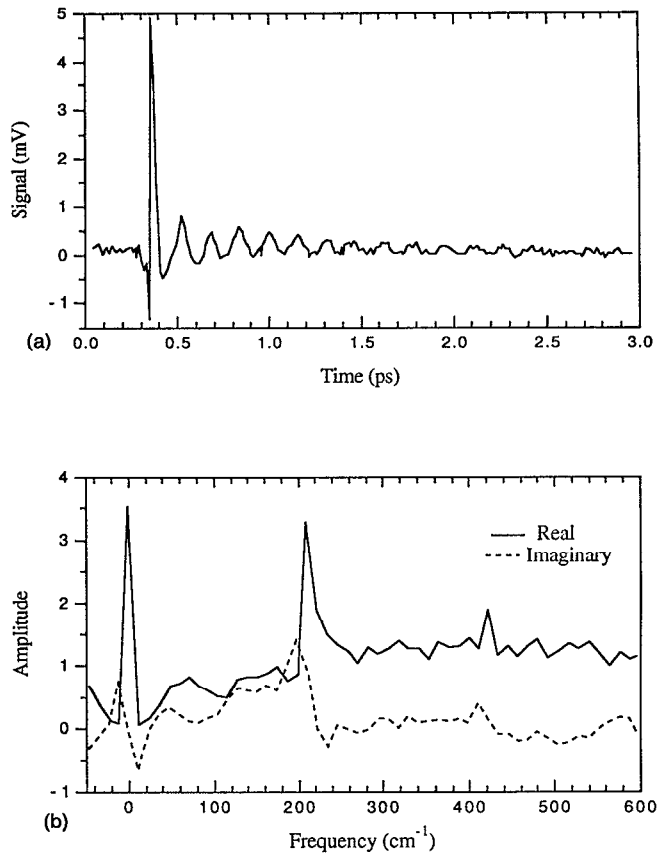

FIG. 15. (a) The resonant OHD dichroism of 5 mM I_2 in *n*-hexane pumped and probed by 30 fs pulses at 580 nm and (b) the Fourier transforms of this response. Solvent bands are not observed in the resonant dichroic responses.

of the resonance secondary radiation spectrum is proportional to the imaginary part of $\wp^3$ derived from just a single density matrix evolution diagram (pathway I). No such interferences contribute to the spontaneous Raman spectrum. Hence both the resonant solute and the nonresonant solvent contribute, weighted by their respective number densities, to the imaginary part of the third order polarization of the solution and thus the resonance Raman spectrum. The interfering polarization components are a function of the capability of ultrafast pulses to directly prepare vibrational coherences.

IV. CONCLUSION

The relative magnitudes of the resonant and nonresonant OHD birefringent and dichroic responses pumped and probed by ultrafast pulses are determined by the constructive or destructive interferences between contributing density matrix time evolution histories. When the pump–probe frequencies are in a region of optical transparency (nonresonant), the birefringent response is on the order of 10–100 times stronger than the dichroic response due to constructive and destructive interference respectively, between third order polarization time evolution pathways. The relative phasing of these time evolution pathways is essentially reversed for electronically resonant chromophores and short pulses. Thus, constructive interferences occur for the resonant dichroic response and destructive interferences contribute to the resonant birefringent intramolecular responses. No such interferences contribute to the cross section of cw Raman scattering due to the monochromatic character of the excitation.

The pulse width and detuning controls the extent of this interference effect and contributes to a small constant phase shift to all ground state responses in the fast pulse limit (pulse width < resonant optical dephasing time). Hence, the relative magnitudes of the dichroic and birefringent responses when the electronically resonant pulse duration is shorter than all other material dephasing times are pulse width dependent. The resonant birefringent responses nearly vanishes for the shortest pulse durations, i.e., when the complex third-order polarization amplitude is almost entirely real. Analogously, in the fast optical dephasing limit, the relative strength of the resonant birefringent and dichroic responses and the t_d independent phase shift of these nuclear responses are controlled by the relative magnitudes of the optical dephasing time constant and the vibrational period (ground or excited state response). When molecular responses are dominated by ex-

cited state dynamics, i.e., $T_2 > \omega_{if}^{-1}$, the resonant birefringent response also vanishes.

The electronically resonant or nonresonant birefringence and dichroism are proportional to the imaginary and real parts of the complex total (i.e., sum over all density matrix histories) third order polarization amplitude, $\wp^3(t)$, respectively. In contrast, the observed spontaneous (or stimulated) Raman scattering spectrum is proportional to just the imaginary part of $\wp^3(t)$. A more complete picture of the vibrational nuclear response function may be provided by a comparison of the birefringent and dichroic responses which are respectively proportional to the imaginary and real parts of the nuclear response function at least for some off-resonant samples.

The comparison of time and frequency domain analysis of nonresonant Raman vibrational resonances leads to a satisfying confirmation of theory but raises questions about the practical significance of nonresonant two-pulse pump–probe studies of intramolecular modes particularly. A Fourier transform of the OHD ground state vibrational response time dependence is shown to be proportional to the anisotropic part of the Raman scattering tensor, i.e., the depolarized light scattering spectrum. In accordance with theory, the nonresonant birefringence of chloroform is found to decay with the same time constant (1.4 ps) that corresponds to the observed depolarized spontaneous Raman scattering bandwidth. Furthermore, the relative contributions of the two low frequency $CHCl_3$ intramolecular modes (262 and 365 cm^{-1}) is identical to that observed in the spontaneous Raman spectrum. To the best of our knowledge this is the most rigorous comparison of a time and frequency domain analysis of Raman resonances. Although the vibrational dephasing time and relative intensities agreement is satisfying, *these femtosecond nonresonant birefringence measurements reveal no new information about intramolecular ground state modes as compared with the Raman frequency domain analysis.* However, this nonresonant OHD birefringent technique is of great value for the direct observation of very low frequency collective, intermolecular and rotational reorientational motions which are much more difficult to observe in frequency domain spectral analysis. Furthermore it remains to be seen whether OHD nonresonant birefringence observations with even shorter pulses may more easily resolve nonexponential decays than the corresponding depolarized Raman spectrum.

However, an advantage of these time domain experiments as compared to frequency domain, i.e., spontaneous Raman scattering that this analysis illustrates, is that the low frequency contribution from the nonresonant solvent, which can often dominate the resonance Raman spectrum of a solution, is missing in the OHD dichroic responses. Thus those low frequency intra- and intermolecular degrees of freedom coupled to the resonant chromophore in a solution may be more clearly observed via time domain measurements than frequency domain studies.

The treatment described here has been limited to a three or four molecular level description, in the absence of inhomogeneous broadening, excited and probed by identical pulses (one-color pump–probe). The extension of this path specific approach to include more sophisticated vibronic and vibrational response functions, as well as the effects of electronic and vibrational inhomogeneities, and two-color pump–probe responses can be readily incorporated. More detailed and quantitative calculations of the relative (and absolute) magnitudes and phases of the resonant birefringence and dichroism of real molecular systems, such as the previously reported I_2,[13] results will depend on a multiexcited state level description which includes cross terms. A more complete treatment of nonresonant responses should also include those density matrix time histories excluded here by the RWA.

Finally, both ground and excited state dynamics are shown here to contribute to the initial phase and magnitude of the ground and excited state nuclear responses. A subsequent wave packet treatment will more explicitly show how the dynamics on the various electronic state surfaces accounts for the relative phase and magnitudes of these responses.

ACKNOWLEDGMENTS

The support of the National Science Foundation is gratefully acknowledged. We thank Professor Graham Fleming for experimental facilities and support that resulted in the time-domain measurements reported here.

APPENDIX

When the pump and probe pulse durations are less than the optical dephasing time of the resonant electronic transition, $\tau < T_2$, the magnitudes of the OHD birefringent and dichroic responses are dependent on the complex integral $G(\Delta)L(\Delta')$ where

$$G(\Delta)L(\Delta') = \int_{-\infty}^{\infty} dt\, e^{-t^2/2\tau^2} e^{i\Delta t} \int_{-\infty}^{t} dt'\, e^{-t'^2/2\tau^2} e^{i\Delta' t'}. \tag{A1}$$

The real and imaginary parts of this expression can be approximated for near resonant short pulse excitation by expanding the exponentials in Eq. (A1). For the integral over t', $[L(\Delta')]$, we have upon expanding $e^{i\Delta' t'}$ up to terms third order in t'

$$\begin{aligned}\mathrm{Re}\, L(\Delta') &= \int_{-\infty}^{t} dt'\, e^{-t'^2/2\tau^2}(1-\Delta'^2 t'^2/2) \\ &= \frac{\Delta'^2\tau^2}{2} te^{-t^2/2\tau^2} + (1-\Delta'^2\tau^2/2)[(\pi/2)^{1/2}\tau \\ &\quad + \sqrt{2}\tau e^{-t^2/2\tau^2}\{(t/\sqrt{2}\tau) + 2(t/\sqrt{2}\tau)^3/1\cdot 3 \\ &\quad + 2^2(t/\sqrt{2}\tau)^5/1\cdot 3\cdot 5 + \cdots\}], \end{aligned} \tag{A2}$$

$$\begin{aligned}\mathrm{Im}\, L(\Delta') &= \int_{-\infty}^{t} dt'\, e^{-t'^2/2\tau^2}(\Delta' t' - \Delta'^3 t'^3/6) \\ &= -\Delta'\tau^2 e^{-t^2/2\tau^2}(1-\Delta'^2 t^2/6 - \Delta'^2\tau^2/3). \end{aligned} \tag{A3}$$

When the $\exp(i\Delta t)$ factor of $G(\Delta)$ is similarly expanded to the t^3 term and Eqs. (A2) and (A3) are substituted in Eq. (A1) we have

$$\mathrm{Re}\{G(\Delta)L(\Delta')\}$$
$$= \int_{-\infty}^{\infty} dt\, e^{-t^2/2\tau^2}[(1-\Delta^2t^2/2)\mathrm{Re}\,L(\Delta') - (\Delta t-\Delta^3t^3/6)\mathrm{Im}\,L(\Delta')], \quad \text{(A4)}$$

$$\mathrm{Im}\{G(\Delta)L(\Delta')\}$$
$$= \int_{-\infty}^{\infty} dt\, e^{-t^2/2\tau^2}[(1-\Delta^2t^2/2)\mathrm{Im}\,L(\Delta') + (\Delta t-\Delta^3t^3/6)\mathrm{Re}\,L(\Delta')]. \quad \text{(A5)}$$

When the expressions for the real and imaginary parts of $L(\Delta')$ are substituted into Eq. (A4), the real part of $G(\Delta)L(\Delta')$ is given by

$$\mathrm{Re}\{G(\Delta)L(\Delta')\}$$
$$= \int_{-\infty}^{\infty} dt\, e^{-t^2/\tau^2}\Big\{\Delta\Delta'\tau^2[t-\Delta^2t^3/6][1-\Delta'^2t^2/6 - \Delta'^2\tau^2/3] + (1-\Delta^2t^2/2)\Big[\frac{\Delta'^2\tau^2}{2}\tau + (1-\Delta'^2\tau^2/2) \times((\pi/2)^{1/2}\tau e^{-t^2/2\tau^2} + t + t^3/3\tau^2 + t^5/15 + \cdots)\Big]\Big\}. \quad \text{(A6)}$$

Only even powers of t make nonzero contributions to this integral, thus we simply have

$$\mathrm{Re}\{G(\Delta)L(\Delta')\} = \int_{-\infty}^{\infty} dt\, e^{-t^2/2\tau^2}(1-\Delta^2t^2/2) \times(1-\Delta'^2\tau^2/2)(\pi/2)^{1/2}\tau = (1-\Delta'^2\tau^2/2)(1-\Delta^2\tau^2/2)\pi\tau^2. \quad \text{(A7)}$$

The imaginary part of this expression can be given as the sum of four contributions

$$\mathrm{Im}\{G(\Delta)L(\Delta')\} = I_1+I_2+I_3+I_4, \quad \text{(A8)}$$

$$I_1 = \int_{-\infty}^{\infty} dt\, e^{-t^2/2\tau^2}\,\mathrm{Im}\,L(\Delta') = \pi^{1/2}\tau^3\Delta'(-1+5\Delta'^2\tau^2/12), \quad \text{(A8a)}$$

$$I_2 = -\frac{\Delta^2}{2}\int_{-\infty}^{\infty} dt\, e^{-t^2/2\tau^2}t^2\,\mathrm{Im}\,L(\Delta') = \frac{\pi^{1/2}\tau^5\Delta^2\Delta'}{4}(1-7\Delta'^2\tau^2/12), \quad \text{(A8b)}$$

$$I_3 = \Delta\int_{-\infty}^{\infty} dt\, e^{-t^2/2\tau^2}t\,\mathrm{Re}\,L(\Delta') = \pi^{1/2}\tau^3\Delta(1-\Delta'^2\tau^2/4), \quad \text{(A8c)}$$

$$I_4 = -\frac{\Delta^3}{3}\int_{-\infty}^{\infty} dt\, e^{-t^2/2\tau^2}t^3\,\mathrm{Re}\,L(\Delta') = -\frac{5\pi^{1/2}\tau^5\Delta^3}{12}(1-21\Delta'^2\tau^2/60). \quad \text{(A8d)}$$

Thus for the imaginary part of $G(\Delta)L(\Delta')$ these terms may be reorganized as

$$\mathrm{Im}\{G(\Delta)L(\Delta')\}$$
$$= \pi^{1/2}\tau^3(\Delta-\Delta')\Big[\Big(1-\frac{\Delta^2\tau^2}{2}\Big)\Big(1-\frac{\Delta'^2\tau^2}{2}\Big) + \frac{(\Delta-\Delta')^2\tau^2}{12} - \frac{5}{48}\Delta^2\Delta'^2\tau^4\Big] \quad \text{(A9)}$$
$$\simeq \pi^{1/2}\tau^3(\Delta-\Delta')(1-\Delta^2\tau^2/2)(1-\Delta'^2\tau^2/2). \quad \text{(A10)}$$

Equation (A10) results when $\Delta\tau<1$ and $\Delta'\tau<1$ as taken here. Thus, the relative magnitudes of the real and imaginary parts of this two-time pulse integral is given in the fast pulse limit by

$$\frac{\mathrm{Im}\,G(\Delta)L(\Delta')}{\mathrm{Re}\,G(\Delta)L(\Delta')} \simeq \frac{\tau}{\pi^{1/2}}(\Delta-\Delta'). \quad \text{(A11)}$$

It should also be noted that the real part of $G(\Delta)L(\Delta')$ will always be a positive quantity while the sign of the imaginary part of $G(\Delta)L(\Delta')$ will depend on $(\Delta-\Delta')$.

[1] W. R. Lambert, P. M. Felker, and A. H. Zewail, J. Chem. Phys. **75**, 5958 (1981); P. M. Felker and A. H. Zewail, Chem. Phys. Lett. **102**, 113 (1983).
[2] J. Chaiken, M. Gurnick, and J. D. McDonald, J. Chem. Phys. **74**, 106 (1981); J. Chaiken and J. D. McDonald, *ibid.* **77**, 669 (1982).
[3] A. Mokhtari, A. Chebira, and J. Chesnoy, J. Opt. Soc. Am. B **7**, 1551 (1990).
[4] S. DeSilvestri, J. G. Fujimoto, E. P. Ippen, E. B. Gamble, Jr., L. R. Williams, and K. A. Nelson, Chem. Phys. Lett. **116**, 146 (1985); Y.-X. Yan, E. B. Gamble, Jr., and K. A. Nelson, J. Chem. Phys. **83**, 5391 (1985); Y.-X. Yan and K. A. Nelson, *ibid.* **87**, 6257 (1987).
[5] S. Ruhman, A. G. Joly, and K. A. Nelson, IEEE J. Quant. Electron. **24**, 460 (1988).
[6] M. J. Rosker, F. W. Wise, and C. L. Tang, Phys. Rev. Lett. **57**, 321 (1986).
[7] F. W. Wise, M. J. Rosker, and C. L. Tang, J. Chem. Phys. **86**, 2827 (1987).
[8] J. J. Gerdy, M. Dantus, R. M. Bowman, and A. H. Zewail, Chem. Phys. Lett. **171**, 1 (1990).
[9] H. L. Fragnito, J.-Y. Bigot, P. C. Becker, and C. V. Shank, Chem. Phys. Lett. **160**, 101 (1989).
[10] D. McMorrow, W. T. Lotshaw, and G. A. Kenney-Wallace, IEEE J. Quant. Electron. **QE-24**, 443 (1988).
[11] J. Chesnoy and A. Mokhtari, Phys. Rev. A **38**, 3566 (1988); A. Mokhtari and J. Chesnoy, Europhys. Lett. **5**, 523 (1988).
[12] T. Hattori, A. Terasaki, T. Kobayashi, T. Wada, A. Yamada, and H. Sasabe, J. Chem. Phys. **95**, 937 (1991).
[13] N. F. Scherer, L. D. Ziegler, and G. R. Fleming, J. Chem. Phys. **96**, 5544 (1992).
[14] M. Cho, S. J. Rosenthal, N. F. Scherer, L. D. Ziegler, and G. R. Fleming, J. Chem. Phys. **96**, 5033 (1992).
[15] Y. J. Yan, L. E. Fried, and S. Mukamel, J. Phys. Chem. **93**, 8149 (1989).
[16] S. Mukamel, Ann. Rev. Phys. Chem. 646 (1990).
[17] Y. J. Yan and S. Mukamel, Phys. Rev. A **41**, 6485 (1990).
[18] L. E. Fried and S. Mukamel, J. Chem. Phys. **93**, 3063 (1990).
[19] M. Cho, G. R. Fleming, and S. Mukamel, J. Chem. Phys. **98**, 5314 (1993).
[20] A. M. Walsh and R. F. Loring, Chem. Phys. Lett. **160**, 299 (1989).

[21] D. Lee and A. C. Albrecht, in *Advances in Infrared and Raman Spectroscopy*, Vol. 12, edited by R. J. H. Clark and R. E. Hester (Wiley, Heyden, 1985), p. 179.
[22] J. S. Melinger and A. C. Albrecht, J. Chem. Phys. **84**, 1247 (1986); J. Phys. Chem. **91**, 2704 (1987).
[23] S. Mukamel, J. Chem. Phys. **82**, 5398 (1985).
[24] J. R. Andrews, R. M. Hochstrasser, and H. P. Tromsdorff, Chem. Phys. **62**, 87 (1981); Y. Prior, A. R. Bogdan, M. Dagenais, and N. Bloembergen, Phys. Rev. Lett. **46**, 111 (1981); A. R. Bogdan, M. W. Downer, and N. Bloembergen, Phys. Rev. A **24**, 623 (1981).
[25] M. Mitsunaga and C. L. Tang, Phys. Rev. A **35**, 1720 (1987); I. A. Walmsley, M. Mitsunaga, and C. L. Tang, *ibid.* **38**, 4681 (1988).
[26] W. T. Pollard, C. H. Brito Cruz, C. V. Shank, and R. A. Mathies, J. Chem. Phys. **90**, 199 (1989).
[27] W. T. Pollard, S.-Y. Lee, and R. A. Mathies, J. Chem. Phys. **92**, 4012 (1990).
[28] G. L. Eesley, M. D. Levenson, and W. M. Tolles, IEEE J. Quant. Electr. **QE-14**, 45 (1978).
[29] M. D. Levenson and S. S. Kano, *Introduction to Nonlinear Laser Spectroscopy* (Academic, San Diego, 1988).
[30] Y. R. Shen, *The Principles of Nonlinear Optics* (Wiley, New York, 1984).
[31] R. W. Hellwarth, Prog. Quant. Electr. **5**, 1 (1977).
[32] F. J. Bartoli and T. A. Litovitz, J. Chem. Phys. **56**, 404 (1972); **56**, 413 (1972)